ISSN 1029-9599, Physical Mesomechanics, 2020, Vol. 23, No. 4, pp. 291–300. © Pleiades Publishing, Ltd., 2020.
Russian Text © The Author(s), 2019, published in Fizicheskaya Mezomekhanika, 2019, Vol. 22, No. 4, pp. 5–15.

Deposition of Cermet Coatings on the Basis of Ti, Ni, WC, and B_4C by Cold Gas Dynamic Spraying with Subsequent Laser Irradiation

V. M. Fomin[1]*, A. A. Golyshev[1], V. F. Kosarev[1], A. G. Malikov[1], A. M. Orishich[1], and A. A. Filippov[1]

[1] *Khristianovich Institute of Theoretical and Applied Mechanics, Siberian Branch, Russian Academy of Sciences, Novosibirsk, 630090 Russia*
** e-mail: fomin@itam.nsc.ru*

Received July 17, 2019, revised July 17, 2019, accepted July 31, 2019

Abstract—This paper studies the formation of cermet coatings by a combined additive manufacturing technology on the basis of cold gas dynamic spraying and subsequent laser irradiation. The coatings are made of titanium and nickel metal powders with ceramic particles of tungsten carbide and boron carbide. Optimal energy parameters are determined for coating deposition by cold gas dynamic spraying and subsequent laser irradiation for powder compositions with different ceramic particles. The microstructure of deposited coatings is studied, and their mechanical properties are measured. It is shown that the combined method of cold gas dynamic spraying and laser irradiation can be used to produce a single-layer cermet coating up to 1 mm thick by sequentially depositing a mixture of powders of different composition, such as B_4C–Ni, B_4C–Ti, WC–Ti. Based on the obtained experimental data, a technique is proposed for a layer-by-layer deposition of thick (≈4 mm) cermet coatings of composition 40% WC + 60% (0.94Ti + 0.06Al) by cold gas dynamic spraying and subsequent laser irradiation.

Keywords: additive manufacturing technologies, cold gas dynamic spraying, laser irradiation, coating, microstructure, roughness, morphology

DOI: 10.1134/S1029959920040025

1. INTRODUCTION

The increasing need for highly functional, lightweight parts of complex geometry has stimulated the rapid growth of additive technologies [1, 2, etc.]. Additive technologies provide a means for production of parts from metals, alloys, polymers, and ceramics. Development of new materials and production technologies of complex parts that have unique operational characteristics and can endure high thermal and mechanical loads is one of the urgent tasks of the modern rocket and space equipment, mechanical engineering, metallurgy, automotive, medical, electronic industries.

Composite materials with a gradient distribution of physical and mechanical properties have been long used in various technical fields. Their use expands due to advances in production technologies of tailored materials for optimal operation in various constructions. Metal-matrix composite coatings are applied to improve product characteristics. Currently, several types of metal-matrix composite coatings have been developed, which are based on Al, Ti, Fe, Cu, Mg, Ni and reinforced with ceramic fibers or microparticles [3].

Coatings formed of Ni-based alloys are widely used to improve the characteristics of such products as turbines, wear-resistant plates, and mill rolls [4–6]. A reserve for increasing the wear resistance of the coatings can be the design of compositions reinforced with carbides. An example is tungsten carbide WC, which has high wear resistance in combination with high heat resistance and good wettability by molten metal [7, 8].

The design of titanium composites opens up the prospect of improving the specific stiffness and high-temperature strength and reducing abrasive wear [9, 10]. TiB is recognized as one of the most efficient reinforcing materials for titanium [11, 12]. Cermet composites based on ceramic compounds B_4C, TiC,

TiB, TiB_2 and the titanium binder yield high operational characteristics due to their high compatibility, increased melting point, extreme hardness, excellent wear and corrosion resistance, and fracture toughness.

At present, no physical and mathematical models and methods exist that can determine microstructural and mechanical characteristics of the product from process characteristics and properties of deposited materials. No correlation has been found between laser parameters, fractional and chemical compositions of powders, and thermophysical characteristics. Therefore, the search for physical laws governing the formation of a monolithic structure with no pores and minimum surface roughness is an urgent task.

A common additive manufacturing technology is selective laser melting (SLM). During laser melting, a focused laser beam moves along a predetermined path, heating particles of the powder bed. The material within the laser spot melts, and a small molten pool is formed, which solidifies upon cooling. Then, a new layer is deposited, and the laser scanning process is repeated until a 3D product is formed. Characteristics of melting of the material and pool formation depend on a number of parameters, such as laser power, scanning speed, beam size, layer thickness, and others.

The combined technology—cold gas dynamic (CGD) spraying [13, 14] and layer-by-layer laser melting—opens up new possibilities for additive technologies. This approach allows a formation of a powder layer with minimum porosity on the surface of any curvature. Papers [15, 16] report the results on laser post-treatment of CGD-sprayed coatings made of titanium alloy and stainless steel.

In the present paper, we propose the complex approach including cold gas dynamic spraying and intensive laser irradiation, which allows a formation of functionally gradient heterogeneous layers of different thickness from ceramic particles WC, B_4C and the metal binder in the form of nickel and titanium powder.

The proposed approach was used to form metal-matrix composite coatings based on Ni, Ti and ceramics B_4C, WC. For CGD-sprayed cermet coatings of different composition, laser parameters (power and scanning speed) are optimized to ensure minimum roughness of melt tracks and to avoid balling in the weld bead and pore formation.

2. EXPERIMENTAL PROCEDURE

Cold gas dynamic spraying of composite coatings of the "metal matrix + ceramic inclusions" type was performed using abrasive powders B_4C with the median particle size $d_{50} = 2$, 9, 44, 64, and 75 μm and WC with $d_{50} = 20$ μm. The metal components are Ni powder PNK-UT-1 and titanium powder PTOM-1. The analysis of volume distribution of powder particles is performed using the LS 13 320 laser diffraction particle size analyzer (Beckman Coulter, USA).

The Venus FTLMV-02 V-shaped mixer is used to prepare powder mixtures with the ceramic mass concentration 10–90%. Substrates are plates made of titanium alloy VT-20 measuring $50 \times 50 \times 5$ mm^3. Coatings are sprayed using the feed-control device and axially symmetrical ceramic Laval nozzle. The CGD-sprayed coatings are treated with a continuous CO_2 laser of power up to 5 kW and wavelength 10.6 μm.

Laser irradiation using a ZnSe lens with a focal length of 304 mm is normally focused, underfocused, and overfocused. The focus position Δf is –20, 0, +20 mm from the upper surface of the substrate. Deposition is carried out in shielding helium [16].

Microstructure is studied using a Zeiss EVO MA 15 scanning electron microscope. Microhardness of the obtained composite coatings is measured on cross sections using a DuraScan 50 automatic microhardness tester (Emco-Test, Austria) and a Wilson Hardness Group Tukon 1102 microhardness tester with a load of 100–300, 500 g by Vickers test. Microhardness is measured at 10 points spaced at 100 μm intervals along a straight line parallel to the surface in the middle of the coating thickness. The obtained microhardness data are averaged.

3. EXPERIMENTAL STUDY OF CERMET TRACKS

3.1. Experimental Study of Cermet Tracks of a B_4C–Ni Powder Mixture

The efficiency of cold gas dynamic spraying for deposition of cermet composite coatings is studied on B_4C powder with the average particle size $d_{50} =$ 43.9 μm and Ni powder PNK-UT-1 with $d_{50} = 12.2$ μm. These powders are used to prepare mechanical Ni–B_4C powder mixtures with the mass fractions of boron carbide from 0.1 to 0.9.

The experiment shows that the spraying coefficient decreases with increasing B_4C concentration in the powder mixture from 0.63 for pure nickel (Fig. 1) to zero for 0.9 wt % B_4C.

Figure 2 shows typical structures of CGD-sprayed cermet coatings viewed in the scanning electron microscope with the backscattered electron detector. By varying particle size of the ceramics, its proportion in

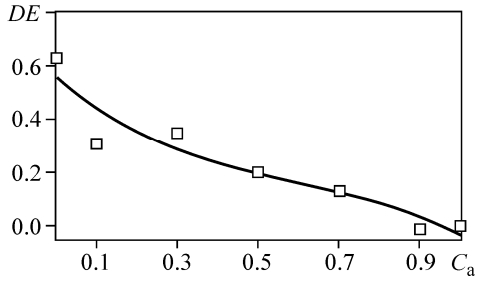

Fig. 1. Spraying coefficient *DE* of the Ni + B_4C powder mixture versus the mass content of the abrasive component C_a. Squares stand for experimental values, the line corresponds to approximation.

the mixture, and the layer thickness, features of the resulting laser coating are studied.

The EDX analysis of the chemical composition demonstrates that spraying of small particles is low efficient and hardly depends on the initial concentration of ceramics. The variation in the initial weight fraction of B_4C ceramics from 30 to 50% increases the real concentration in the coating from 19.92 to 20.99%.

The study of the coating morphology depending on the laser focus position Δf at different mass content and size of ceramics in the initial mixture (Fig. 3) reveals a strong influence of the B_4C content on the track shape. Three modes are distinguished: cladding (the track is higher than the CGD-sprayed coating, with a convex meniscus in the center), flat mode (the track is level with the coating), and penetration (the track is lower than the CGD-sprayed coating, with a concave meniscus in the center). The track structure depends on both the size of the B_4C particles and their concentration.

The main contribution to the track shape is evidently made by convective mass transfer in contrast to diffusive mass transfer in the mechanism of formation of track structure and volume distribution of ceramic particles. Convection is caused and forced by the surface tension gradient. In laser heating, the material temperature is maximum in the beam center and decreases to its edges. The surface tension of a liquid (melt) depends on the temperature and usually decreases with its growth. This gives rise to a force directed from the center of the light spot to its edges and inducing the liquid motion, resulting in a cylindrical concave meniscus. This is the case at a low concentration and small size of ceramic particles. However, with a large concentration of coarse particles of 30Ni70B_4C (Fig. 3) the temperature dependence of the tension coefficient alternates in sign, which results in a convex cylindrical meniscus at the ceramic particle size $d_{50} = 64$ and 75 μm. In this case, a fairly smooth cylindrical surface with the small roughness $R_a \approx 3$ is formed, which is significantly less (approximately 4 times) than the roughness of the track at a low ceramic content. At the B_4C powder size $d_{50} = 44$ μm (Fig. 2), the melt surface is practically flat, which indicates a weak temperature dependence of the surface tension coefficient. An important consequence of the convective motion of the melt is the

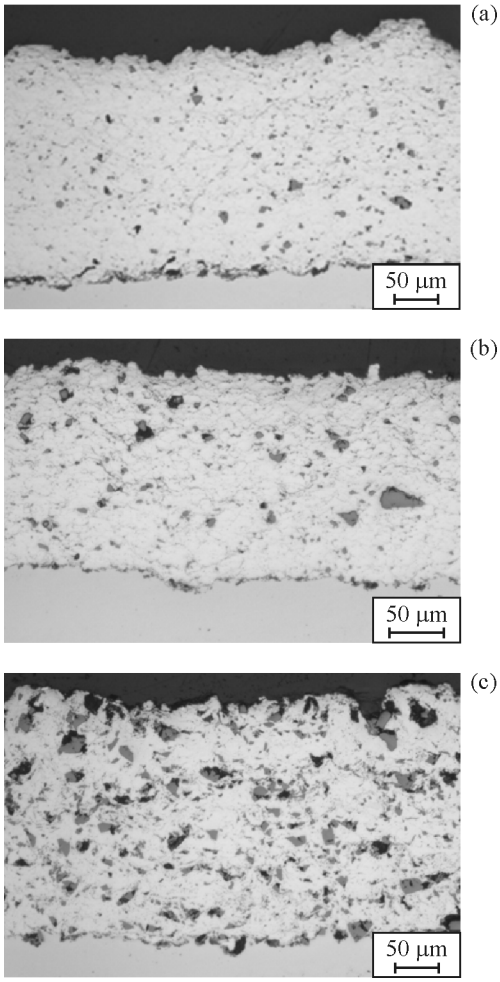

Element	wt %	Element	wt %	Element	wt %
B	19.92	B	20.99	B	37.46
C	28.23	C	25.23	C	25.74
Ni	51.65	Ni	53.46	Ni	35.85
Other	Fe (0.20)	Other	Fe (0.32)	Other	Si (0.12) Fe (1.14)
Total	100	Total	100	Total	100

Fig. 2. Microphotos of cross sections and chemical composition of CGD-sprayed Ni/B_4C coatings (a–c) with the B_4C mass content 30 (a), 50 (b), 70% (c) and particle size $d_{50} = 2.9$ (a, b) and 75 μm (c).

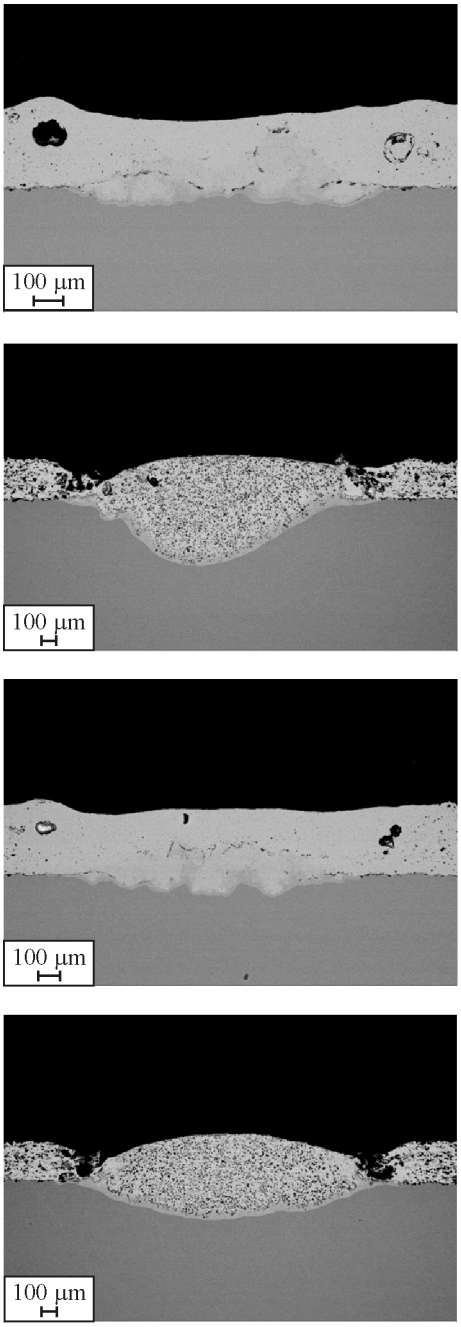

Fig. 3. EDX image of cross sections of laser tracks at different B_4C particles: 30% B_4C, 70% Ni, d_{50} = 2.9 μm (a, c), 70% B_4C, 30% Ni, d_{50} = 75 μm (b, d); Δf = –20 mm (a, b), Δf = +20 mm (c, d).

accumulation of pores at the lateral boundaries of the track (Fig. 3).

By studying the track width and depth, it was found that the penetration depth and width grow at higher ceramic content in the initial mixture. When the particle size within the track is comparable to that outside the track, it is apparent that laser irradiation of the CGD-sprayed coating causes B_4C particles to refine as well as to mix in the track.

Table 1. Spectral analysis (with reference to Fig. 4)

Elements	Spectrum No.				
	1	2	3	4	5
B	8.83	10.31	17.98	29.75	9.94
C	8.17	10.22	10.65	12.85	9.73
Ni	3.15	25.23	8.11	1.99	41.89
Ti	71.89	48.74	60.95	55.41	33.85
Other	Al (5.79) V (1.28) N (1.18)	Al (3.66) Fe (0.72) N (1.12)	Al (1.01) V (1.29)	0	Al (2.47) N (0.79) Fe (1.33)

Optimization of the laser modes illustrates that high-quality single tracks with minimum roughness at the maximum content of B_4C ceramics (d_{50} = 44 μm) in the CGD-sprayed coating, which are level with the coating, can be formed at the laser power 0.6 kW, speed 0.4 m/min, and Δf = +20 mm. The optimum thickness of the CGD-sprayed coating is under 2 mm. This concentration is chosen to form a multilayer coating.

A detailed study of the chemical composition of the track shows that laser irradiation of the CGD-sprayed 70Ni30B_4C coating changes the material composition (Table 1) and size of solid inclusions (Fig. 4).

Dark aggregates are found to contain 55.41 wt % Ti and 29.95 wt % B. Light gray aggregates exhibit an increased Ti content (71.89%). The solid solution consists of Ti (48.47%) and Ni (25.23%). There are also elongated light gray aggregates with Ti (66.77%), Ni (2.06%), and B (19.72%). A significant amount of

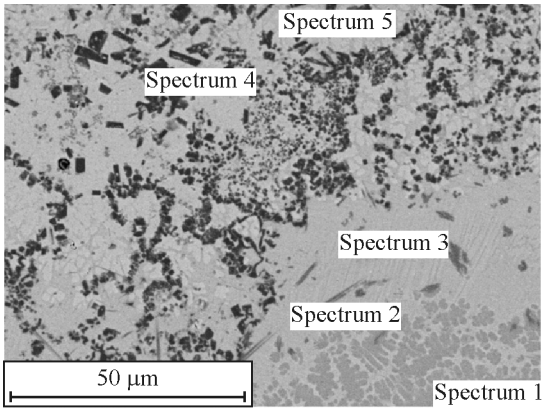

Fig. 4. Cross-sectional view of the structure of a track formed in the CGD-sprayed coating of the 70Ni30B_4C powder mixture.

titanium is additionally transferred from the substrate to the track.

The process of laser deposition of a powder based on Ni and boron carbide B–C on the titanium substrate was previously studied [4–8]. Meng et al. used only fine ceramics (3–5 μm) in an amount of 5% by weight mixed with the nickel-based powder with the particle sizes 50–80 μm [4]. A 0.8 mm layer of the powder mixture with an organic binder (polyvinyl alcohol and water) was spread over the surface of the Ti–6Al–4V substrate. A transfer of titanium from the substrate was shown to lead to an active reaction: TiB_2 crystals were formed. A similar change in the ceramics composition is assumed to occur in a CGD-sprayed 70Ni30B_4C coating with a fine ceramic powder $d_{50} = 2.9$ μm. However, in coatings including B_4C with fractions 44 and 64 μm (Fig. 5), coarse particles apparently do not have time to completely react during the melt existence, but their size decreases significantly.

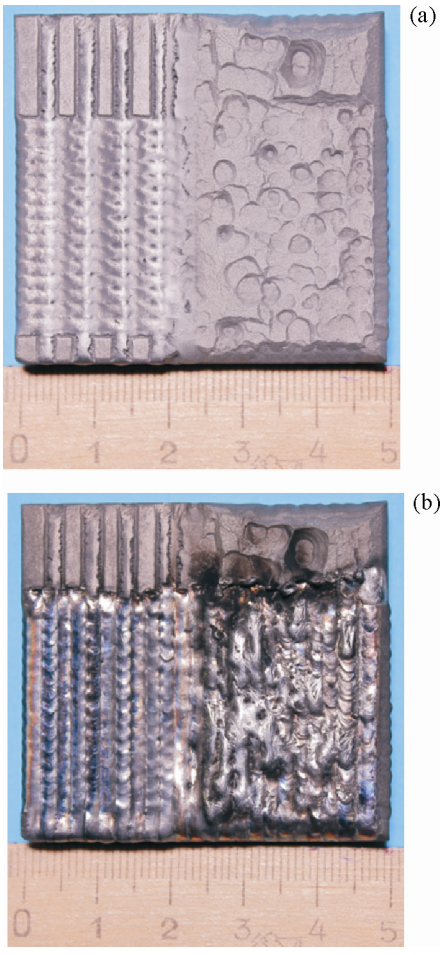

Fig. 5. Third layer of the CGD-sprayed coating (a) and arrays of laser tracks (b) (color online).

3.2 Experimental Study of a Multilayer Cermet Coating of the B_4C–Ni Powder Mixture

The study of the single-layer coating deposition reveals an important feature of formed tracks: accumulation of defects in the form of pores at the lateral edges. This feature inherent in a single track is preserved for track arrays. For coarse ceramic particles, and consequently at the negative gradient of the surface tension coefficient, the melt beneath the surface moves to the edges together with various defects; on the surface, from the pool walls to the track axis. In this case, almost all pores remain on the edge. For a low concentration and fine particles of B_4C, the reverse occurs. The molten material in the center rises from depth, and on the surface it is forced to the pool edges. In this case, some pores remain on the surface and in the bulk, which degrades the deposited layer quality.

From profilograms of high-quality track arrays, optimal laser modes and track spacing h are determined for CGD-sprayed coatings of the thickness 200 μm, 0, 5, and 1 mm with the mixture composition 30% Ni, 70% B_4C, $d_{50} = 44$ μm. Then, the second layer of the CGD-sprayed coating is deposited. Scanning pattern is both cross and consecutive relative to previous tracks. Table 2 presents optimal laser modes for CGD-sprayed coatings of different thicknesses.

When the coating is thicker than 2 mm, craters appear on the surface. This reduces the spraying coefficient for the coating thicker than 4 mm due to a decreased angle of impact of particles with steep walls of these craters, which is inversely proportional to the spraying coefficient. Craters are also found at the junctions of laser tracks of the CGD-sprayed coatings. Porosity at the track boundaries opens due to sanding or during cold gas dynamic spraying and becomes the nucleus for a crater that grows in the CGD-sprayed coating formed by the next layer. Laser irradiation of such coatings increases the surface roughness. The characteristic structure of the multilayer coating is shown in Fig. 5.

Table 2. Optimal modes of laser irradiation of CGD-sprayed coatings 30% Ni, 70% B_4C

Thickness of the CGD-sprayed coating, mm	W, kW	V, m/min	Δf, mm	h, mm
0.2	0.6	0.4	+20	1.0
0.5	2.0	0.4	–20	2.0
1.0	2.0	0.5	–2	2.8

4. EXPERIMENTAL STUDY OF THE CERMET COATING B_4C–Ti + Al

For high-quality thick multilayer coatings, titanium powder PTOM-1 is used as the metal matrix, with aluminum powder being added in some cases. The introduction of the aluminum powder into the initial mixture is explained in Sect. 5.

Based on the procedure described in Sect. 3, multilayer cermet structures 0.6–4.0 mm thick are formed. Modes of cold gas dynamic spraying of thick coatings based on titanium and boron carbide are determined for various content of boron carbide in the initial mixture, as well as optimal laser modes are found. Typical photos of the obtained coatings are shown in Fig. 6. Optimal laser modes are achieved at the laser power 1 kW, speed 0.7 m/min, track spacing 1.25 mm, and focus position 9 mm from the upper surface of the CGD-sprayed 3-mm-thick coating. The spot size is approximately 1.5 mm in this case.

For a CGD-sprayed coating of thickness 0.6 mm and the powder composition 30% Ti : 70% B_4C, the laser modes are optimized (W = 1.5 kW, speed 0.4 m/min, focus position +20 mm, track spacing 2 mm) to obtain high-quality track arrays with minimum roughness.

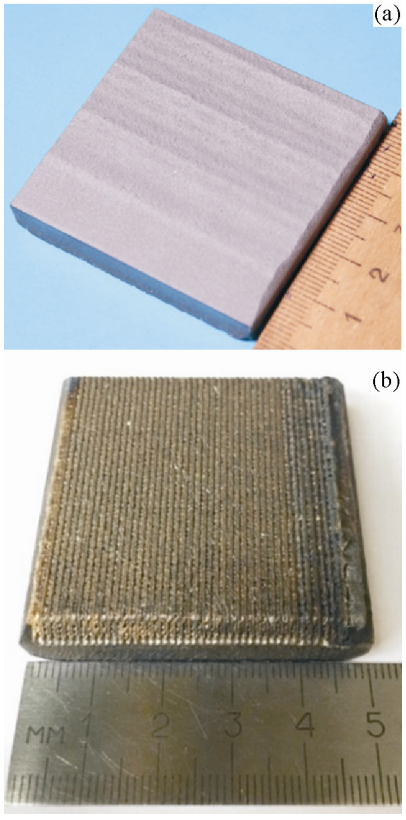

Fig. 6. CGD-sprayed coating before (a) and after laser irradiation (b) (color online).

A CGD-sprayed 1-mm-thick coating is formed of 30Ti70B_4C, the ceramic size d_{50} = 64 μm. Variation in laser modes (W = 0.5–2.0 kW, V = 0.5–1.0 m/min) and focus position fails to provide high-quality single tracks. The structure of track arrays shows that at the focus position +20 mm the penetration depth is ≈300 μm for the coating thickness 1 mm. The increased penetration depth due to the focus position in the knife mode degrades the track array surface and consequently the quality of deposition of the next layer of CGD-sprayed coating. As in the case of the Ni matrix, the structure of single tracks depends on the B_4C particles. At the B_4C particle size d_{50} = 64 μm and the concentration 30% Ti, 70% B_4C in the 0.6-mm-thick coating, penetration occurs, i.e. the track is lower than the CGD-sprayed coating, the meniscus in the center is concave (Fig. 7a). However, for the Ni matrix, the meniscus is convex (Fig. 3) at the same ceramic size and concentration in the initial mixture. At the optimal track spacing 2 mm, the array structure is close to the structure of a single track (Fig. 7b). Concave menisci complicate the deposition of the second layer of the cermet coating based on Ti and B_4C.

Figure 8 shows the characteristic microstructure of a cross section of the multilayer coating 70% B_4C + 30% (0.94Ti + 0.06Al). Table 3 shows the concentration of chemical elements (wt %) in the coating 70% B_4C + 30% (0.94Ti + 0.06Al).

It is known that thermal action on the mixture of titanium and boron carbide gives an exothermic reaction $3Ti + B_4C = TiC + 2TiB_2$ [17–21]. From Fig. 7 and Table 3, it can be assumed that ceramic particles of boron carbide dissolve in the coating being formed (the initial size 75 μm). Here, the prolonged aggregates are titanium carbide whiskers, and the hexagonal

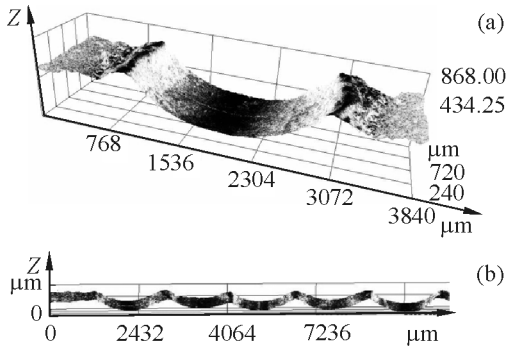

Fig. 7. Profilogram of the single track (a) and array of tracks (b) of 30% Ti, 70% B_4C specimens. The ceramics measures d_{50} = 64 μm.

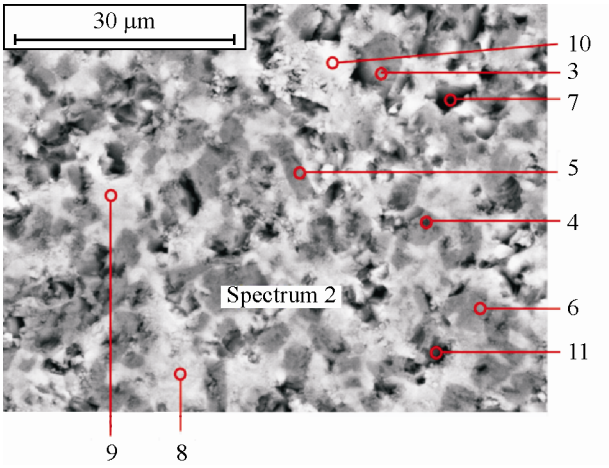

Fig. 8. EDX analysis of the cermet structure 70% B_4C + 30% (0.94Ti + 0.06Al) (color online).

aggregates are titanium diboride, which result from internal synthesis due to laser irradiation of the CGD-sprayed cermet coating.

High-quality thick multilayer cermet coatings are also formed of ceramics WC (d_{50} = 10–20 μm) and the metal matrix in the form of PTOM-1 grade titanium powder.

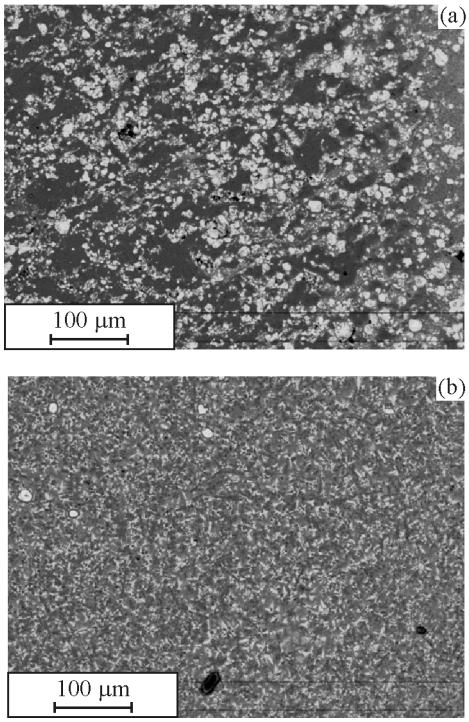

Fig. 9. Cross-sectional view of the structure of the multilayer coating 40% WC + 60% (0.94Ti + 0.06Al). CGD-sprayed coating (a), array of tracks (b).

5. EXPERIMENTAL STUDY OF MULTILAYERED CERMET COATINGS WC–Ti + Al

Modes are developed for cold gas dynamic spraying of coatings from WC–Ti mixtures. For these coatings, laser irradiation is optimized to obtain high-quality single tracks and its arrays.

When pure Ti is used as the binder, tracks have an important feature: formation of droplets of solidified metal between them, i.e. balling. For CGD-sprayed coatings based on PTOM-1 grade pure Ti, droplets do not completely disappear by varying the track spacing or laser energy parameters. The presence of droplets greatly complicates the formation and preparation of a high-quality second layer of the CGD-sprayed cermet coating composed of Ti powder PTOM-1 (30%) and WC powder (70%). High-quality thick multilayer coatings are obtained if the 94% Ti and 6% Al powder mixture is used as the metal matrix.

Modes of cold gas dynamic spraying of 2-mm-thick coatings from the 40% WC + 60% (0.94Ti + 0.06Al) powder mixture are developed. Laser energy parameters are optimized (W = 1.2 kW, V = 0.8 m/min, Δf = –20 mm, spacing 1 mm). Based on the obtained experimental data, a technique is deve-

Table 3. Chemical composition of the 70% B_4C + 30% (0.94Ti + 0.06Al) coating

Elements	Spectrum No.									
	2	3	4	5	6	7	8	9	10	11
B	37.90	35.88	38.43	38.55	35.46	11.79	25.68	14.57	16.05	35.38
C	4.58	5.95	4.69	9.36	5.65	1.62	7.39	4.29	7.52	5.94
Al	0.14	4.30	0.34	0.65	0.76	0.22	2.06	7.75	5.15	0.34
Ti	57.38	53.72	56.55	51.44	57.94	86.37	63.80	65.69	63.34	58.34
O		0.15					0.37	6.45	6.23	
Other					P (0.19)		Si (0.17) P (0.37) Fe (0.27) Cu (0.26)	Si (0.26) Fe (0.33) Cu (0.37)	Si (0.28) P (0.4) Fe (0.49) Cu (0.56)	

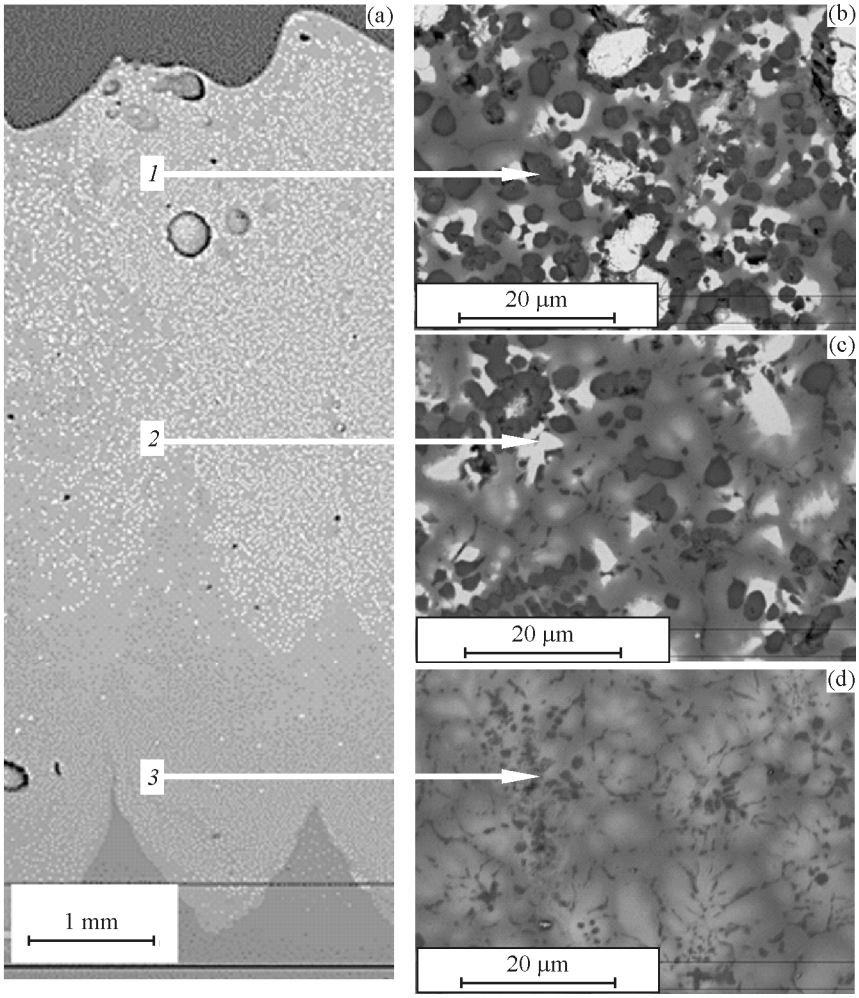

Fig. 10. Cross-sectional view of the structure of the multilayer coating deposited by successive CGD spraying and laser irradiation, thickness 4 mm, 40% WC + 60% (0.94Ti + 0.06Al).

loped for layer-by-layer growing of thick (≈4 mm) cermet coatings based on 40% WC + 60% (0.94Ti + 0.06Al) (Figs. 9 and 10).

The structural morphology of the track and CGD-sprayed coating shows a uniform distribution of WC particles (Fig. 9). In the CGD-sprayed coating, the tungsten carbide concentration is close to the initial one. After laser irradiation of the CGD-sprayed coating, the WC particles refine as compared to the particles in the CGD-sprayed coating (Fig. 9).

To study the microstructure, chemical composition, macrohardness of a 4-mm-thick multilayer coating, three zones are distinguished (Fig. 10a). The chemical composition differs in the zones (Table 4).

The morphology of the multilayer coating structure varies in height. In the multilayer coating, various ag-

Table 4. Chemical composition of the coating in different zones

Element	Upper zone (1)		Middle zone (2)		Lower zone (3)	
	wt %	at %	wt %	at %	wt %	at %
C K	8.30	34.13	8.39	32.57	7.14	26.91
Al K	2.39	4.37	3.17	5.51	4.14	6.94
Ti K	49.19	50.67	54.57	53.32	63.43	59.92
W M	40.12	10.83	33.86	8.60	25.31	6.23
Total	100.00		100.00		100.00	

Table 5. Microhardness values $HV_{0.1}$

	Coating material			
	70Ni30B_4C	50Ni50B_4C	30Ni70B_4C	
CGD spraying	225	250	278	
CGD spraying + laser irradiation	313	756	1117	
VT20 substrate, center				330

gregates—from light to dark—are observed in the solid solution. The light aggregate is tungsten carbide. The dark aggregate is a compound of Ti (78.63%), W (11.91%), and C (8.82%) in weight concentration. The solid solution consists of the following elements: Ti (52.32%), W (37.39%), C (6.80%), and Al (3.5%). The dark aggregate is titanium carbide. In the upper zone, the light and dark aggregates prevail in the solid solution. In the middle zone, the aggregates are uniformly distributed in the solid solution. The lower zone contains predominantly the solid solution.

The concentration of carbon C and aluminum Al remains nearly the same in all the zones. The concentration of titanium increases from 49.19 to 59.92% with depth. The opposite situation occurs for the tungsten concentration, which decreases from 40.12 to 25.31% with depth. Laser irradiation of the mixture leads to the formation of various carbides in the coating, but, in contrast to B_4C ceramics, the surface quality of tracks and track arrays does not degrade, which makes it possible to apply subsequent high-quality layers by cold gas dynamic spraying.

The developed technique enables a formation of thick heterogeneous materials of composition 40% WC + 60% (0.94Ti + 0.06Al) by a successive deposition of the powder by cold gas dynamic spraying and subsequent laser irradiation.

6. MECHANICAL CHARACTERISTICS

For cermet structures to develop, we study how microhardness depends on the thickness, volume concentration and material of ceramics in the mixture. Of particular interest is the hardness due to laser irradiation of the coating of a cermet powder mixture. Table 5 shows microhardness values averaged over 10 measurements for the substrate, CGD-sprayed coating, and CGD-sprayed and laser-irradiated coating of the NiB_4C mixture at different ceramic concentrations at a load of 100 g.

Table 6. Microhardness values

Material	Substrate	CGD-sprayed coating	CGD-sprayed and laser-irradiated coating
	Microhardness $HV_{0.3}$		
70% B_4C + 30% (Ti + Al)	327.5	466.3	1331.3
	Microhardness $HV_{0.1}$		
40% WC + 60% (0.94Ti + 0.06Al)	330	520	620

With the NiB_4C mixture, the microhardness increases as the B_4C content grows in the initial mixture. Laser treatment of the CGD-sprayed coating with coarse particles of boron carbide can improve the microhardness by 3–4 times to the value $HV_{0.1}$ = 1117 MPa. Table 6 presents the microhardness values for the 70% B_4C + 30% (Ti + Al) mixture at a load of 300 g and the 40% WC + 60% (0.94Ti + 0.06Al) mixture at a load of 100 g.

The microhardness of the CGD-sprayed coating of composition B_4C + (Ti and Al) is $466.3HV_{0.3}$ and increases to $1331.3HV_{0.3}$ after laser treatment.

With tungsten carbide WC, laser irradiation slightly changes the microhardness of the CGD-sprayed coating ($HV_{0.1}$ = 520 and 620, respectively).

7. CONCLUSIONS

The conditions were determined for formation of high-quality single tracks and multilayer coatings depending on the laser power, scanning speed, and beam width at the maximum volume content of B_4C and WC in CGD-sprayed coatings. The possibility of forming a single-layer cermet coating up to 1 mm in thickness by gas dynamic spraying of a powder mixture of various compositions B_4C–Ni, B_4C–Ti, WC–Ti, WC–Ni and subsequent laser melting was shown.

The effect of the powder composition and size, amount of the deposited material on the efficiency of cold gas dynamic spraying, microstructure, porosity, roughness, and microhardness of the coating before and after laser irradiation was analyzed. Of particular interest was the hardness due to laser irradiation of the coating of a cermet powder mixture. For the cermet structure of the initial mixture 40% WC + 60% (0.94Ti + 0.06Al), laser irradiation gives on average the microhardness $620HV_{0.1}$. The CGD-sprayed coating of composition B_4C + (Ti and Al) has the microhardness 466.3, which increases to $1331.3HV_{0.3}$ after laser treatment. This can be associated with the formation of TiC and TiB_2 ceramics due to internal synthesis induced by laser irradiation of the CGD-sprayed cermet coating.

For the $30Ni70B_4C$ mixture, the microhardness was $1117HV_{0.1}$ after laser melting, which is 4 times higher than that of the CGD-sprayed coating ($278HV_{0.1}$).

For WC particles, the microhardness of the CGD-sprayed coating ($HV_{0.1}$ = 520) is slightly different from that of the laser-irradiated structure ($HV_{0.1}$ = 620).

Considerable study was given to multilayer structures. It was found that a material after laser melting has high microhardness and significant surface rough-

ness. These parameters determine high heterogeneity of the second and subsequent CGD-sprayed coatings, which degrades the surface quality at subsequent laser treatment.

Based on the obtained experimental data, a technique is proposed for a layer-by-layer deposition of thick (≈4 mm) cermet coatings of composition 40% WC + 60% (0.94Ti + 0.06Al) by cold gas dynamic spraying and subsequent laser irradiation, in which the microhardness of the laser tracks is close to that of the cold sprayed coating.

FUNDING

This work was supported by the Russian Science Foundation grant No. 16-19-10300.

REFERENCES

1. Choong, Y.C., Maleksaeedi, S., Eng, H., Wei, J., and Su, P., 4D Printing of High Performance Shape Memory Polymer Using Stereolithography, *Mater. Des.*, 2017, vol. 126, pp. 219–225.
2. Gan, M. and Wong, C., Properties of Selective Laser Melted Spodumene Glass-Ceramic, *J. Eur. Ceram. Soc.*, 2017, vol. 37, no. 13, pp. 4147–4154.
3. Miracle, D.B., Metal Matrix Composites from Science to Technological Significance, *Compos. Sci. Technol.*, 2005, vol. 65, pp. 15–16.
4. Meng, Q.W., Geng, T.L., and Zhang, B.Y., Laser Cladding of Ni-Base Composite Coatings onto Ti–6Al–4V Substrates with Pre-Placed B_4C + NiCrBSi Powders, *Surf. Coat. Technol.*, 2006, vol. 200, pp. 4923–4928.
5. Chaliampalias, D., Vourlias, G., Pavlidou, E., Skolianos, S., Chrissafis, K., and Stergioudis, G., Comparative Examination of the Microstructure and High Temperature Oxidation Performance of NiCrBSi Flame Sprayed and Pack Cementation Coatings, *Appl. Surf. Sci.*, 2009, vol. 255, p. 3605.
6. Guo, C., Zhou, J., Chen, J., Zhao, J., Yu, Y., and Zhou, H., High Temperature Wear Resistance of Laser Cladding NiCrBSi and NiCrBSi/WC-Ni Composite Coatings, *Wear*, 2011, vol. 270, no. 7–8, pp. 492–498.
7. Tobar, M., Alvarez, C., Amado, J., Rodriguez, G., and Yanez, A., Morphology and Characterization of Laser Clad Composite NiCrBSi–WC Coatings on Stainless Steel, *Surf. Coat. Technol.*, 2006, vol. 200, pp. 6313–6317.
8. Bonny, K., Baets, P., Vleugels, J., Huang, S., and Lauwers, B., Dry Reciprocating Sliding Friction and Wear Response of WC-Ni Cemented Carbides, *Tribol. Lett.*, 2008, vol. 31, no. 3, pp. 199–209.
9. Pouzet, S., Peyre, P., Gorny, C., Castelnau, O., Baudin, T., Brisset, F., Colin, C., and Gadaud, P., Additive Layer Manufacturing of Titanium Matrix Composites Using the Direct Metal Deposition Laser Process, *Mater. Sci. Eng. A*, 2016, vol. 677, pp. 171–181.
10. Cai, C., Song, B., Qiu, C., Li, L., Xue, P., Wei, Q., Zhou, J., Nan, H., Chen, H., and Shi, Y., Hot Isostatic Pressing of In-Situ TiB/Ti–6Al–4V Composites with Novel Reinforcement Architecture, Enhanced Hardness and Elevated Tribological Properties, *J. Alloys Comp.*, 2017, vol. 710, pp. 364–374.
11. Saito, T., Furuta, T., and Yamaguchi, T., *Development of Low Cost Titanium Alloy Matrix Composites, Recent Advances in Titanium Metal Matrix Composites*, Froes, F.H. and Storer, J., Eds., Rosemont: Illinois, 1994.
12. Ravi Chandran, K.S., Panda, K.B., and Sahay, S.S., TiB_w-Reinforced Ti Composites: Processing, Properties, Application Prospects, and Research Needs, *JOM*, 2004, vol. 56, no. 5, pp. 42–48.
13. Alkhimov, A.P., Kosarev, V.F., Fomin, V.M., and Klinkov, S.V., *Cold Gas Dynamic Spraying. Theory and Applications*, Moscow: Fizmatlit, 2010.
14. Fomin, V.M., Golyshev, A.A., Kosarev, V.F., Malikov, A.G., Orishich, M.A., Ryashin, N.S., Filippov, A.A., and Shikalov, V.S., Creation of Heterogeneous Materials on the Basis of B_4C and Ni Powders by the Method of Cold Spraying with Subsequent Layer-by-Layer Laser Treatment, *J. Appl. Mech. Tech. Phys.*, 2017, vol. 58, no. 5, pp. 947–955.
15. Marrocco, T., Hussain, T., Mccortney, D.G., and Shipway, P., Corrosion Performance of Laser Posttreated Cold Sprayed Titanium Coatings, *J. Therm. Spray Technol.*, 2011, vol. 20, pp. 909–917.
16. Sova, A., Grigoriev, S., Okunkova, A.A., and Smurov, I., Cold Spray Deposition of 316L Stainless Steel Coatings on Aluminium Surface with Following Laser Post Treatment, *Surf. Coat. Technol.*, 2013, vol. 235, pp. 283–289.
17. Tang, J., Mechanical and Tribological Properties of the TiC-TiB_2 Composite Coating Deposited on 40Cr-Steel by Electrospark Deposition, *Appl. Surf. Sci.*, 2016, vol. 365, pp. 202–208. doi 10.1016/j.apsusc.2015.12.198
18. Tijo, D. and Masanta, M., Mechanical Performance of In-Situ TiC-TiB_2 Composite Coating Deposited on Ti-6Al–4V Alloy by Powder Suspension Electro-Discharge Coating Process, *Surf. Coat. Technol.*, 2017, vol. 328, pp. 192–203. doi 10.1016/j.surfcoat.2017.08.048
19. Tijo, D., Masanta, M., and Das, A.K., In-Situ TiC-TiB_2 Coating on Ti-6Al-4V Alloy by Tungsten Inert Gas (TIG) Cladding Method: Part I. Microstructure Evolution, *Surf. Coat. Technol.*, 2018, vol. 344, pp. 541–552. doi 10.1016/j.surfcoat.2018.03.082
20. Tijo, D. and Masanta, M., Effect of Ti/B_4C Ratio on the Microstructure and Mechanical Characteristics of TIG Cladded TiC-TiB_2 Coating on Ti-6Al-4V Alloy, *J. Mater. Proc. Tech.*, 2019, vol. 266, pp. 184–197.
21. Li, J., Yu, Zh., Wang, H., and Li, M., Microstructural Characterization of Titanium Matrix Composite Coatings Reinforced by in Situ Synthesized TiB + TiC Fabricated on Ti6Al4V by Laser Cladding, *Rare Met.*, 2010, vol. 29, no. 5, pp. 465. doi 10.1007/s12598-010-0151-y
22. Tijo, D., and Masanta, M., In-Situ TiC-TiB_2 Coating on Ti-6Al-4V Alloy by Tungsten Inert Gas (TIG) Cladding Method: Part II. Mechanical Performance, *Surf. Coat. Technol.*, 2018, vol. 344, pp. 579–589. doi 10.1016/j.surfcoat.2018.03.082